



HAL
open science

γ' -V 2 O 5 Polymorph: A Genuine Zn Intercalation Material for Nonaqueous Rechargeable Batteries

Ankush Bhatia, Jiahui Xu, Jean-Pierre Pereira-Ramos, Gwenaelle Rouse, Rita Baddour- Hadjean

► **To cite this version:**

Ankush Bhatia, Jiahui Xu, Jean-Pierre Pereira-Ramos, Gwenaelle Rouse, Rita Baddour- Hadjean. γ' -V 2 O 5 Polymorph: A Genuine Zn Intercalation Material for Nonaqueous Rechargeable Batteries. Chemistry of Materials, 2021, 10.1021/acs.chemmater.1c03739 . hal-03504877

HAL Id: hal-03504877

<https://hal.science/hal-03504877>

Submitted on 30 Dec 2021

HAL is a multi-disciplinary open access archive for the deposit and dissemination of scientific research documents, whether they are published or not. The documents may come from teaching and research institutions in France or abroad, or from public or private research centers.

L'archive ouverte pluridisciplinaire **HAL**, est destinée au dépôt et à la diffusion de documents scientifiques de niveau recherche, publiés ou non, émanant des établissements d'enseignement et de recherche français ou étrangers, des laboratoires publics ou privés.

This document is confidential and is proprietary to the American Chemical Society and its authors. Do not copy or disclose without written permission. If you have received this item in error, notify the sender and delete all copies.

The γ' -V₂O₅ Polymorph: a Genuine Zn Intercalation Material for Non-Aqueous Rechargeable Batteries

Journal:	<i>Chemistry of Materials</i>
Manuscript ID	cm-2021-03739n.R2
Manuscript Type:	Article
Date Submitted by the Author:	n/a
Complete List of Authors:	Bhatia, Ankush; Institut de Chimie et des Matériaux Paris-Est, Xu, Jiahui; Institut de Chimie et des Matériaux Paris-Est Pereira-Ramos, Jean-Pierre; Institut de Chimie et des Matériaux Paris-Est, Institut de Chimie et des Matériaux Paris Est Rousse, Gwenaëlle; College de France, UMR8260 Baddour-Hadjean, Rita; Institut de Chimie et des Matériaux Paris-Est,

SCHOLARONE™
Manuscripts

The γ' -V₂O₅ Polymorph: a Genuine Zn Intercalation Material for Non-Aqueous Rechargeable Batteries

Ankush Bhatia¹, Jiahui Xu¹, Jean-Pierre Pereira-Ramos¹, Gwenaëlle Rousse², Rita Baddour-

*Hadjean^{*1}*

¹ Institut de Chimie et des Matériaux Paris Est (ICMPE), UMR 7182 CNRS-Université Paris Est

Créteil (UPEC), 2, rue Henri Dunant, F-94320, Thiais, France

² Chimie du Solide-Energie, UMR 8260 CNRS-Sorbonne Université, Collège de France 75231

Paris, France

**corresponding author: baddour@icmpe.cnrs.fr*

Abstract

The electrochemical properties of the puckered layered γ' -V₂O₅ polymorph as cathode material in a non-aqueous Zn-metal cell using acetonitrile-Zn(CF₃SO₃)₂ electrolyte are investigated here for the first time. The typical galvanostatic profile in the 2 V- 0.3 V vs. Zn²⁺/Zn voltage range shows

1
2
3
4 a sloping discharge curve involving a capacity of 130 mAh g⁻¹ at C/20 in one single step centered
5
6
7 at 0.9 V vs. Zn²⁺/Zn. The structural response of γ' -V₂O₅ during the discharge-charge cycle is
8
9
10 investigated by *ex-situ* X-ray diffraction (XRD) and Raman spectroscopy. Up to 0.41 Zn mol⁻¹ can
11
12
13 be accommodated between the γ' -V₂O₅ layers, inducing only a moderate interlayer expansion of
14
15
16 +6.4%, comparable to that found for Li⁺ insertion. Remarkably, the insertion process is fully
17
18
19 reversible in spite of the high charge density of Zn²⁺. Good cycle life can be achieved at moderate
20
21
22 rate, with a stable capacity of nearly 130 mAh g⁻¹ available at 0.9 V vs Zn²⁺/Zn over at least 60
23
24
25 cycles. The peculiar structural features of the new electroformed Zn_{0.41}V₂O₅ bronze highlight the
26
27
28 interest of the γ' -V₂O₅ polymorph to mitigate the expected large deformation upon electrochemical
29
30
31 divalent Zn²⁺ incorporation.
32
33
34
35
36
37
38
39
40
41

42 1. Introduction

43
44

45 Lithium Ion Batteries (LIBs) dominate the energy market of portable electronics due to their
46
47
48 high energy density and long cycle life. However, their high costs, toxicity, the scarcity of lithium
49
50
51 and safety issues are strong drawbacks that impede the use of LIBs for large-scale applications
52
53
54
55 such as electric transportations and grid-scale energy storage. In search of alternative batteries,
56
57
58
59
60

1
2
3 aqueous rechargeable Zn-based batteries (ARZB) are quite attractive owing to the high volumetric
4
5
6 and gravimetric capacities delivered by the Zn metal anode (5851 mAh mL⁻¹; 820 mAh g⁻¹), their
7
8
9 low cost, safety and moderate toxicity¹⁻⁴. The major problems of ARZBs are the limited energy
10
11
12 density due to the narrow electrochemical window (1.2 V) as well as the spontaneous dissolution
13
14
15 of MnO₂- and V₂O₅-based cathodes in aqueous electrolytes⁴. The use of non-aqueous electrolytes
16
17
18 would overcome these issues, providing a higher operating voltage of Zn-ion battery and avoiding
19
20
21 dissolution. Various non-aqueous Zn-based electrolytes have recently been reported to work in a
22
23
24 wide electrochemical window (3.8 V vs. Zn²⁺/Zn) such as acetonitrile (AN)-Zn(TFSI)₂, AN-
25
26
27 Zn(CF₃SO₃)₂, and propylene carbonate (PC)-Zn(TFSI)₂ electrolytes⁵. The challenge is to find
28
29
30 cathode materials affording a high working voltage combined with a high-specific capacity.
31
32
33
34
35
36

37 While many papers are devoted to cathode materials for ARZBs such as Prussian blue and
38
39 analogues, manganese oxides and vanadium-based compound^{6,7}, only a few candidates are
40
41 reported for non-aqueous rechargeable Zn batteries (NARZBs)⁸⁻¹⁷. From a pioneering work, the
42
43 electrochemical Zn intercalation in Chevrel-type molybdenum cluster chalcogenides Mo₆X₈ (X =
44
45 S, Se) was found to occur at 0.5 V-0.3 V, using zinc perchlorate in PC or AN electrolyte⁸. In 2000,
46
47
48 the reversible Zn intercalation in β-ZrNCl and related compounds was reported in 0.2 M solution
49
50
51
52
53
54
55
56
57
58
59
60

1
2
3
4 of $\text{Zn}(\text{CF}_3\text{SO}_3)_2$ in a mixture of dimethylsulfoxide (DMSO) and (PC) in a 1:4 volume ratio⁹. More
5
6
7 recently, a Zn/PANi (polyaniline) cell was cycled in a non-aqueous PC-Zn(TFSI)₂ electrolyte¹⁰.
8
9
10 Spinel cathodes $\text{ZnAl}_x\text{Co}_{2-x}\text{O}_4$ and $\text{ZnNi}_x\text{Mn}_x\text{Co}_{2-2x}\text{O}_4$ investigated in AN-Zn(CF_3SO_3)₂^{11,12} were
11
12
13 shown to operate near 1.7-1.8 V, involving attractive capacities of 140-170 mAh g⁻¹. The reversible
14
15
16 Zn insertion has been demonstrated near 1 V in a nanostructured hydrated layered-type birnessite
17
18
19 $\delta\text{-MnO}_2$, leading to a capacity of 100 mAh g⁻¹ without formation of ZnMn_2O_4 spinel upon
20
21
22 cycling¹³. In spite of the richness of their chemical composition and structure, vanadium oxides-
23
24
25 based compounds have been little investigated in NARZBs¹⁴⁻¹⁷. The hydrated layered forms
26
27
28 $\text{V}_3\text{O}_7\cdot\text{H}_2\text{O}$ and $\text{V}_2\text{O}_5\cdot 0.67\text{H}_2\text{O}$ have been reported to deliver interesting stable capacities in the
29
30
31 range 150-200 mAh g⁻¹ at 0.65 V in AN-Zn(CF_3SO_3)₂¹⁵ and 0.9 V in AN-Zn(TFSI)₂¹⁴,
32
33
34 respectively. A freestanding vanadium oxide $\text{V}_2\text{O}_5\cdot 0.14\text{H}_2\text{O}$ -carbon nanotube film has been
35
36
37 recently explored with higher capacity values (≈ 300 mAh g⁻¹) but working at a low potential, near
38
39
40 0.6 V¹⁶. Indeed, water-containing structures constitute one strategy to promote reversible Zn^{2+}
41
42
43 storage¹⁵. The water molecules provide expanded interlayer spacing and are thought to buffer the
44
45
46 charge density of inserted Zn^{2+} cations. Finally, the most common and stable V_2O_5 polymorph, α
47
48
49
50
51 V_2O_5 has been also reported, using a nanosizing strategy. Porous architectures made of 3D V_2O_5
52
53
54
55
56
57
58
59
60

1
2
3
4 nanorods offer also a high reversible capacity of $\approx 300 \text{ mAh g}^{-1}$ near 0.7 V ¹⁷. However, except the
5
6
7 study devoted to $\text{V}_3\text{O}_7 \cdot \text{H}_2\text{O}$ ¹⁵, the structural analysis of the cathode material upon discharge-
8
9
10 charge is overlooked or absent.

11
12
13
14 Such capacity values prompted us to explore the interest of other V_2O_5 polymorphs as cathode
15
16
17 material in NARZB, especially the metastable 2D γ' - V_2O_5 , that is the charge product of the γ -
18
19
20 LiV_2O_5 bronze formed upon electrochemical lithiation of α - V_2O_5 at 2.3 V vs. Li^+/Li ¹⁸. This open
21
22
23 intercalation host with larger interlayer spacing ($\approx 5 \text{ \AA}$ vs. 4.37 \AA for α - V_2O_5) and highly puckered
24
25
26 V_2O_5 stacked layers provides a vast abundance of interlayer interstitial sites. Furthermore, DFT
27
28
29 studies have predicted lower diffusion barriers and higher operating voltage for such cation-free
30
31
32 metastable phases^{19,20}. Indeed, recent experimental studies in our group have demonstrated the
33
34
35 superior electrochemical performance of γ' - V_2O_5 toward $\text{Li}^{+21,22}$, Na^{+23-26} and K^{+27} insertion
36
37
38 compared to α - V_2O_5 ²⁷⁻²⁹. The lithium insertion mechanism in γ' - V_2O_5 was found to involve
39
40
41 reversible and mitigated structural changes consisting in wide solid solution domains²¹ which stand
42
43
44 in contrast to the successive phase transitions required to accommodate Li-ions in the
45
46
47 thermodynamically stable α - V_2O_5 polymorph³⁰. Also, γ' - V_2O_5 was reported to insert almost 1
48
49
50
51
52
53
54
55
56
57
58
59
60

1
2
3
4 Na^{+23–26} and 0.78 K⁺ per mole of oxide²⁷, remarkably at close working voltage to that observed for
5
6
7 Li⁺ insertion (3.3 V vs. Na⁺/Na and 3.1 V vs K⁺/K, respectively).
8
9

10 These attractive results encouraged us to enrich the study of γ' -V₂O₅ intercalation chemistry to
11
12 the case of Zn²⁺ insertion in a non-aqueous electrolyte. Han et al investigated a range of non-
13
14 aqueous electrolytes and clearly indicated AN-Zn(CF₃SO₃)₂ as one of the most suitable for
15
16 reversible cycling of Zn metal anode, providing a wide electrochemical window up to 3.6 V vs.
17
18 Zn²⁺/Zn⁰. In addition, the low viscosity (0.37 mPa s) of AN combined to a dielectric constant of
19
20 36.6 afford fast ionic mobility and high conductivity (17 mS cm⁻¹).
21
22
23
24
25
26
27
28
29

30 Herein, we investigate for the first time the electrochemical properties of the γ' -V₂O₅ polymorph
31
32 in the 2.0 V – 0.3 V voltage range in a Zn-metal cell using AN-Zn(CF₃SO₃)₂ (Zn(OTf)₂)
33
34 electrolyte. The cycling and rate capability properties are reported and the structural response of
35
36 γ' -V₂O₅ upon discharge and charge is explored using *ex-situ* X-ray diffraction (XRD) and Raman
37
38 spectroscopy. We show that γ' -V₂O₅ behaves as a genuine Zn intercalation compound, with the
39
40 electrochemical formation of a new layered γ -type Zn_{0.41}V₂O₅ bronze and a fully reversible
41
42 extraction accompanied by the complete restoration of the pristine oxide structure.
43
44
45
46
47
48
49
50
51
52
53
54
55
56
57
58
59
60

2. Experimental

γ' -V₂O₅ was obtained by the chemical oxidation of γ -LiV₂O₅ synthesized from the chemical lithiation of a fine powder of a α -V₂O₅ precursor prepared by the polyol method³¹. Lithiation of α -V₂O₅ is performed using an excess of lithium iodide in AN to obtain the intermediate δ -LiV₂O₅ phase. A heat treatment at 300°C for 2 h under dynamic primary vacuum in a Büchi® furnace allows the phase transition toward γ -LiV₂O₅. The last step consists in quantitatively extracting Li from γ -LiV₂O₅ by oxidation in a NO₂BF₄ solution (solid Alfa Aesar 96%) in AN (V₂O₅/NO₂BF₄ molar ratio 1/4) under stirring for 24 h at room temperature. After washing with AN and vacuum drying at 70°C for 24 h, the orange γ' -V₂O₅ powder is obtained. Electrochemical titration using galvanostatic oxidation and chemical redox titration confirmed the 5+ oxidation state of vanadium in γ' -V₂O₅.

The pristine powder and the electrodes were characterized by scanning electron microscopy (SEM), (Zeiss, Merlin-type microscope). The elemental compositions were determined from electron dispersive X-ray spectroscopy (EDS) analysis together with SEM using an accelerating voltage of 10 – 15 kV.

1
2
3
4 Crystal structures were characterized by XRD and Raman spectroscopy. XRD experiments were
5
6
7 performed in Bragg-Brentano geometry using a Panalytical XPert pro apparatus equipped with a
8
9
10 X'Celerator detector and Co K α radiation ($\lambda_{K\alpha 1} = 1.78901 \text{ \AA}$, $\lambda_{K\alpha 2} = 1.79290 \text{ \AA}$). The recorded
11
12
13 patterns were refined using the Rietveld method as implemented in the FullProf program^{32,33}.
14
15

16
17 The Raman spectra were recorded with a LaBRAM HR 800 (Jobin-Yvon, Horiba) Raman micro-
18
19
20 spectrometer including edge filters and equipped for signal detection with a back illuminated
21
22
23 charge-coupled device detector (Spex CCD) cooled by the Peltier effect to 200 K. A He-Ne laser
24
25
26 (632.8 nm) was used as the excitation source. The spectra were measured in back-scattering
27
28
29 geometry. To avoid local heating of the sample, the power of the laser beam was adjusted to 0.2 –
30
31
32
33 0.5 mW with neutral filters of various optical densities. The resolution was about 0.5 cm^{-1} . A $100\times$
34
35
36 objective was used to focus the laser light on the sample surface to a spot size of $1 \mu\text{m}^2$.
37
38
39

40
41 Electrochemical experiments were carried out at 20°C using 2032 coin-type cells, which are
42
43
44 assembled in an argon-filled inert atmosphere glovebox ($<0.5 \text{ ppm}$ of H_2O and $<0.5 \text{ ppm}$ of O_2).
45
46
47 The positive electrode was prepared by mixing 80 wt % of active material (about 8 mg) with 7.5
48
49
50 wt % of acetylene black, 7.5 wt % graphite and 5 wt % of PTFE as the binder. Zn metal foil (Alfa
51
52
53 Aesar, $> 99\%$ purity) was used as the negative electrode. The Zn metal surface was polished by
54
55
56
57
58
59
60

1
2
3 using 600-grit sand paper followed by washing with ethanol to remove the surface oxide layer.
4
5

6
7 The two electrodes are separated by a Whatmann glass fiber separator soaked in the non-aqueous
8

9
10 AN- $\text{Zn}(\text{OTf})_2$ 0.3 M electrolyte (AN from Sigma Aldrich > 99.8% purity). The $\text{Zn}(\text{OTf})_2$ powder
11

12
13 was dried overnight at 100°C under vacuum and the AN was dried by keeping it over regenerated
14

15
16 molecular sieves before use. Galvanostatic cycling measurements were performed using a VMP3
17

18
19 Biologic apparatus in the 0.3 V-2 V vs. Zn^{2+}/Zn voltage window at room temperature at different
20

21
22 current densities (147 mA g^{-1} corresponds to 1C).
23
24
25

26
27 The structural investigation was carried out using two electrodes coin cells. The cells were
28

29
30 discharged at C/20 rate up to different x composition in $\text{Zn}_x\text{V}_2\text{O}_5$ ($0 \leq x \leq 0.41$). The highest Zn
31

32
33 content ($x = 0.41$) was attained on fifth discharge at C/20. After 2 h relaxation time, the cells were
34

35
36 disassembled in the glove box. The positive electrodes were rinsed 3 times with AN in order to
37

38
39 remove any electrolyte residue and placed in appropriate airtight sample holders to be further
40

41
42 analyzed by XRD and Raman spectroscopy. Raman spectra were recorded on 10 different spots of
43

44
45 each electrode. Very similar spectra were obtained, regardless of the illuminated spot, indicating
46

47
48 a homogeneous electrochemical reaction in the chosen experimental conditions.
49
50
51
52
53
54
55
56
57
58
59
60

3. Results and discussion

3.1. Structural characterization

The solution technique carried out to synthesize γ' -V₂O₅ leads to a nanosized powder composed of platelets of 500 nm long maximum and ~ 200 nm wide (**Figure 1**). The Rietveld refinement of the XRD pattern (**Figure 2a**) is performed with an initial structural model reported by J. M. Cocciantelli³⁴, and all atoms were freely refined. The final refinement shown in **Figure 2a** indicates that γ' -V₂O₅ crystallizes in an orthorhombic unit cell (*Pnma* space group) with lattice parameter $a = 9.94387(9)$ Å, $b = 3.58389(3)$ Å, $c = 10.03601(9)$ Å in good agreement with previous studies^{18,21,23,26,34}. The structural parameters, including a bond-valence-sum (BVS) analysis³⁵ and V-O bond lengths are gathered in **Tables S1** and **S2**.

The structure of γ' -V₂O₅ (insert in **Figure 2a**) consists of infinite ribbons parallel to the b axis made of VO₅ edges-sharing distorted pyramids oriented alternatively up and down, leading to two non-equivalent vanadium environments. These chains are linked to each other along the a -direction by one pyramid corner oxygen, forming puckered layers perpendicular to the c -axis. The mean crystallite size estimated from diffraction peaks width is 90 – 100 nm.

1
2
3
4 From the local structure point of view, the Raman spectrum of γ' -V₂O₅ (**Figure 2b**) is composed
5
6
7 of 21 peaks in the 90-1050 cm⁻¹ wavenumber range, as previously reported^{36,37}. The projection of
8
9
10 the γ' -V₂O₅ structure along the *b*-crystallographic direction showing all the V–O contacts in the
11
12
13 two vanadium environments (V_a, V_b) is shown in insert of **Figure 2b**. All the vibrations of the
14
15
16 chains can be identified: the stretching of the two shortest V_a-O_{1a} and V_b-O_{1b} bonds at 1037, 1021,
17
18
19 and 1003 cm⁻¹, the bond stretching vibrations localized within the V_a-O₃-V_b bridges at 752 and
20
21
22 603 cm⁻¹, and those of the V_a-O_{2a}-V_a and V_b-O_{2b}-V_b bridges forming the rails of the ladders at
23
24
25 722 and 694 cm⁻¹. Modes involving the longest V–O₂ inter-chains ladder step bonds are observed
26
27
28 at 532 and 500 cm⁻¹, while lower-frequency modes located at 91, 126, 138, 153, 171, 190, 238,
29
30
31 266, 282, 299, 349, and 390 cm⁻¹ are related to the complex distortions of the ladders³⁶.
32
33
34
35
36

37 *3.2. Electrochemical study*

38
39
40 **Figure 3a** shows the cyclic voltammogram (CV) of γ' -V₂O₅ recorded in the 0.3 V- 2 V vs.
41
42
43 Zn²⁺/Zn voltage range at 0.1 mV s⁻¹. The CV curves show one well-resolved broad cathodic peak
44
45
46 centered at ca. 0.96 V while a main peak appears at 1.43 V in oxidation, preceded by a small
47
48
49 contribution around 1 V. The same coulombic charge of 0.64 e⁻ mol⁻¹ is involved during reduction
50
51
52 and oxidation, showing the high reversibility of the electrochemical process. The shape of the CV
53
54
55
56
57
58
59
60

1
2
3
4 curves remains the same on cycling but the efficiency of the electrochemical reaction progressively
5
6
7 improves during the first cycles to reach a maximum value of $\approx 0.8 \text{ e}^- \text{ mol}^{-1}$ after 10 cycles.
8
9

10 The galvanostatic study of $\gamma\text{-V}_2\text{O}_5$ has been performed at C/20 rate ($\approx 8 \text{ mA g}^{-1}$) in the same 0.3
11
12
13 V- 2 V vs. Zn^{2+}/Zn voltage range. As shown in **Figure 3b**, the working potential gradually
14
15
16 decreases during the first discharge, from 1.37 V down to 0.75 V and then in a steeper way in the
17
18
19 last third of the discharge, involving a total faradaic yield of 0.64 F mol^{-1} (specific capacity of 95
20
21
22
23
24
25
26
27
28
29
30
31
32
33
34
35
36
37
38
39
40
41
42
43
44
45
46
47
48
49
50
51
52
53
54
55
56
57
58
59
60
mAh g^{-1}).

Upon subsequent charge of the cell, the potential increases abruptly to stabilize around 1.20 V,
and then significantly increases from the mid-charge up to 2 V. The slightly higher capacity value
recovered in charge is probably due to slight electrolyte decomposition^{12,13} that might be promoted
when using acetylene black-graphite mixture in the composite electrode. Indeed, using another
carbon matrix as carbon nanotubes (CNTs), we have checked this overcharge can be completely
suppressed (**Figure S1**). From cycle 1 to cycle 5 (**Figure 3b**), the capacity continuously increases
from 95 to 130 mAh g^{-1} without any change in the discharge profile. Such electrochemical
phenomenon has already been described elsewhere. It could be attributed to a decrease in the
charge transfer resistance at the negative electrode because of progressive electrochemical

1
2
3 polishing of the Zn surface^{14,15} and/or gradual utilization of active material¹⁷. From the complete
4
5
6 charged state, i.e. from 2 V, the voltage rapidly falls down to ~1.2 V upon discharge, then gives
7
8
9
10 rise to a smooth slope involving the total charge capacity. After this short activation process of a
11
12
13 few cycles, following charge-discharge curves completely superimpose, showing a moderate
14
15
16 sloppy profile with a mid-discharge potential of 0.9 V (**Figure 3c**). Cycling experiments point to a
17
18
19 remarkable retention of the capacity at C/20 over at least 60 cycles at a value of around 120 mAh
20
21
22 g⁻¹ combined with a 100% coulombic efficiency (**Figure 3d**). At 1C, the capacity moderately
23
24
25 decreases by 10%, from 90 to 80 mAh g⁻¹ after 100 cycles (insert of **Figure 3d**).
26
27
28
29

30 The maximum capacity of 130 mAh g⁻¹ here achieved for γ -V₂O₅ is lower than that reported for
31
32
33 the hydrated bilayered V₂O₅·0.67H₂O electrodeposited on carbon foam substrate, with ≈ 200 and
34
35
36 160 mAh g⁻¹ at C/10 and 1C, respectively in 0.5 M Zn(TFSI)₂-AN electrolyte¹⁴. Zn intercalation
37
38
39 into BL(bilayered)-V₂O₅ takes place practically at a slightly lower mid-discharge voltage (≈ 0.8
40
41
42 V). Such reaction seems to be more difficult in the hydrated V₃O₇·H₂O oxide investigated in the
43
44
45 same AN-Zn(CF₃SO₃)₂ 0.25 M electrolyte¹⁵. Indeed, this material delivers about the same capacity
46
47
48 value of 150 mAh g⁻¹ at near 0.65 V, but after at least 30 cycles at C/20, and the first discharge
49
50
51 never exceeds 50 mAh g⁻¹. Remarkable values are exhibited by a freestanding hydrated V₂O₅-CNT
52
53
54
55
56
57
58
59
60

1
2
3 electrode at 0.7C with $\approx 300 \text{ mAh g}^{-1}$ in 1M $\text{Zn}(\text{ClO}_4)_2$ -ethylene carbonate (EC)/ethyl methyl
4
5
6 carbonate (EMC) electrolyte¹⁶. However, this composite electrode rather consists in a model
7
8
9
10 electrode since the carbon matrix is very large (33.7 wt % CNTs). In addition, in the absence of
11
12
13 Zn perchlorate salt heat-treatment, huge capacities might be ascribed to the presence of residual
14
15
16 water molecules in the electrolyte promoting Zn or Zn-proton insertion. A two-electron process is
17
18
19 outlined in the case of 3D nanorods architectures of V_2O_5 ¹⁷ after a quite long activation process of
20
21
22
23 80 cycles at C/3 leading to a capacity of 300 mAh g^{-1} . The authors claim this kind of α -type
24
25
26 nanosized vanadium pentoxide operates as a Zn intercalation compound, which seems doubtful
27
28
29 according to the huge capacitive contribution as high as 30-60% observed in the coulombic charge.
30
31
32

33
34 The C-rate dependence on the galvanostatic cycles (**Figure 4a**) and the discharge capacity
35
36 (**Figure 4b**) of γ' - V_2O_5 have been investigated in the C/20-2C range. At C/20, the capacity
37
38
39 stabilizes near 130 mAh g^{-1} after 5 cycles, indicating the maximum amount of Zn ions insertion-
40
41
42 extraction is close to 0.45 per mol of oxide. Increasing the C rate to C/10, C/5 and C/2 leads to a
43
44
45 progressive capacity decrease to 113, 92 and 85 mAh g^{-1} , respectively, which corresponds to 87%,
46
47
48 71% and 65% of the maximum value, respectively. At 1C and 2C, the capacity nearly does not
49
50
51 decline, with 80 mAh g^{-1} still available at 2C. The present rate capability performance is slightly
52
53
54
55
56
57
58
59
60

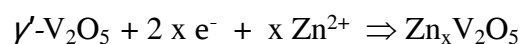
1
2
3 lower than that reported for the hydrated bilayered BL-V₂O₅ cathode in 0.5 M Zn(TFSI)₂-AN
4
5
6
7 electrolyte with still 80% and 70% of the maximum capacity available at 1C and 5C, respectively¹⁴.
8
9

10 However, as shown in **Figure 4b**, the cell completely recovers the initial capacity of 120 mAh g⁻¹
11
12
13 when subsequently operated at C/20, which indicates the structure of the cathode has not been
14
15
16
17 damaged by applying 2C rate. Finally, a high reversibility of the discharge-charge process and
18
19
20 excellent capacity stability are achieved, regardless of the applied C rate.
21
22

23
24 The electrochemical behavior at room temperature of the conventional α -V₂O₅ polymorph has
25
26
27 been also investigated in the same AN-Zn(CF₃SO₃)₂ 0.3 M electrolyte for comparison. **Figure S2a**
28
29
30 shows the cyclic voltammetric curves achieved for the two polymorphs. The coulombic charge
31
32
33 involved in the case of α -V₂O₅ is only \approx 20% that achieved for γ' -V₂O₅. From galvanostatic curves
34
35
36 obtained at C/20 (**Figure S2b**), Zn insertion in α -V₂O₅ takes place around 0.7 V vs. Zn²⁺/Zn V, i.
37
38
39 e. 200 mV lower than γ' -V₂O₅, which indicates a much more difficult reaction. The major
40
41
42 distinctive feature lies in a greatly lower capacity for α -V₂O₅, rapidly stabilizing around only 30
43
44
45 mAh g⁻¹ (**Figures S2b-S2c**). The superior working voltage and higher capacity found for γ' -V₂O₅
46
47
48 illustrate once again the advantage of this open structure toward Zn²⁺ intercalation, as previously
49
50
51 demonstrated in the case of monovalent alkali ions insertion^{21,23,27}.
52
53
54
55
56
57
58
59
60

3.3. Structural changes during the electrochemical process

In order to get insight into the Zn reaction mechanism, several γ' -V₂O₅ electrodes have been prepared at various depths of discharge and charge (0.12 to 0.82 F mol⁻¹) at C/20 rate and further analyzed by XRD and Raman spectroscopy. **Table 3** summarizes the electrodes history and results of EDS analysis. Zn element is systematically detected by EDS, with a good accord between the expected Zn content and the faradaic yield, assuming the following intercalation process:



Indeed, the Zn content in V₂O₅ evaluated from EDS fits remarkably that calculated from coulombic charge (see **Table 3**). The negligible Zn amount of 0.02 achieved after the first charge is probably due to residual Zn traces in spite of the rinsing procedure.

The *ex-situ* XRD patterns of the Zn_xV₂O₅ discharged electrodes (x = 0.06, 0.13, 0.19, 0.25, 0.32 and 0.41) are gathered in **Figure 5a**. Upon Zn insertion, the γ' -V₂O₅ peaks progressively decrease in intensity and shift toward lower angle peaks, indicating that Zn insertion occurs through a solid solution region in the whole 0 ≤ x ≤ 0.41 composition range, in good agreement with the electrochemical profile showing a characteristic sloping curve (**Figure 3b**). The diffraction pattern of the Zn_{0.41}V₂O₅ phase can be indexed with the same *Pnma* space group of the γ' -V₂O₅ pristine

1
2
3 material, with unit cell parameters of $a = 9.9053(7) \text{ \AA}$, $b = 3.60501(20) \text{ \AA}$, $c = 10.6822(9) \text{ \AA}$
4
5
6
7 indicating an expansion of the c lattice parameter, which suggests Zn^{2+} cations are likely placed
8
9
10 between the γ' - V_2O_5 layers.

11
12
13 The *ex-situ* Raman spectra of the discharged $\text{Zn}_x\text{V}_2\text{O}_5$ electrodes ($x = 0.06, 0.13, 0.19, 0.25, 0.32$
14 and 0.41) are gathered in **Figure 5b**. One can see that the Raman spectra keep the original features
15
16
17 of the pristine material, but with a loss of intensity and band broadening indicating the emergence
18
19
20 of some disorder in the plane of the V_2O_5 chains upon Zn insertion. In the high wavenumber range,
21
22
23 of some disorder in the plane of the V_2O_5 chains upon Zn insertion. In the high wavenumber range,
24
25
26 the shift of the apical $\text{V}=\text{O}$ stretching modes toward frequencies lower than 1000 cm^{-1} suggests a
27
28
29 lengthening of these bonds upon V^{5+} to V^{4+} reduction. For the most reduced electrodes ($x = 0.32$
30
31
32 and 0.41), a new broad band at $\approx 884 \text{ cm}^{-1}$ is observed, which can be assigned to the symmetric
33
34
35 stretching vibration of the VO_3 group, as commonly reported for many vanadate minerals³⁸.
36
37
38

39
40 Hence, the main effect of Zn intercalation in γ' - V_2O_5 consists in an interlayer expansion by 6.4%
41
42
43 (from 10.04 \AA to 10.68 \AA) while the a and b in-plane parameters undergo negligible changes. As
44
45
46 a result, the unit cell volume increases by the same 6.4% factor, from 358 \AA^3 for the pristine oxide
47
48
49 to 381 \AA^3 for the electroformed $\text{Zn}_{0.41}\text{V}_2\text{O}_5$ bronze (**Figure 6**). The moderate interlayer dilation of
50
51
52
53 6.4% induced by Zn accommodation is comparable to that observed upon Li^+ insertion (6%, see
54
55
56
57
58
59
60

1
2
3
4 **Table 2)**²¹, probably because of the small size of Zn²⁺ (ionic radius of 0.74 Å vs. 0.76 Å for Li⁺).
5
6
7 Differently, sodium insertion in γ' -V₂O₅ was proved to induce a huge dilation of 18%^{23,24} while
8
9
10 only a 10% expansion was reported for K⁺ insertion²⁷ due to the important polarizability of
11
12
13 potassium. Hence, it appears the size and polarizability of the guest cation in γ' -V₂O₅ control the
14
15
16 magnitude of the interlayer expansion. The V₂O₅ layers puckering along the *a* axis is very limited
17
18
19 in the case of Zn insertion (0.4%) compared to lithiation (2.6%)²¹ and sodiation (1.7%)²³,
20
21
22 suggesting that the charge of the guest cation would mitigate the puckering effect. Finally, the *b*
23
24
25 parameter increases by 0.5%, which is in good accord with the previous evolution of 0.5% and 1%
26
27
28 found for lithiation and sodiation, respectively. It is also consistent with a diffusion of Zn ions
29
30
31 along the *b* direction.
32
33
34
35

36
37 The structural reversibility upon charge and cycling experiments has been examined by XRD
38
39
40 and Raman spectroscopy. Comparison of the fingerprints of the pristine electrode and that after
41
42
43 one cycle (**Figure 7**) clearly shows the typical XRD pattern and Raman spectrum of γ' -V₂O₅ are
44
45
46 recovered, indicating that highly reversible structural change takes place upon oxidation. After 60
47
48
49 cycles, the initial structure is recovered with however some intensity decrease and peaks
50
51
52 broadening pointing to some disordering process.
53
54
55
56
57
58
59
60

3.4. Characterization of the electroformed $Zn_{0.41}V_2O_5$ bronze

The formation of the $Zn_{0.41}V_2O_5$ bronze from electrochemical reduction of γ' - V_2O_5 at room temperature is reported here for the first time. Indeed, high temperature reaction of Zn on α - V_2O_5 at 630°C leads to the poor Zn containing bronze $Zn_{0.03}V_2O_5$ whose structure is close to the parent oxide α - V_2O_5 . Another vanadium bronze with a higher Zn content, ξ - $Zn_{0.26-0.29}V_2O_5$, has been reported without any structural determination^{39,40}. The thermal treatment of an appropriate nitrate-sucrose mixture lead to the formation of a layered nanostructured $Zn_{0.29}V_2O_5$ ⁴¹. The latter is also indicated as a discharge product of V_2O_5 nanosheets on hierarchical TiN nanowire arrays in an aqueous rechargeable Zn-ion battery⁴². For higher Zn/V ratio values, for instance 0.5, 1 and 1.5, ZnV_2O_6 , $Zn_2V_2O_7$ and $Zn_3V_2O_8$ vanadates with structural features very far from those found for the present $Zn_{0.41}V_2O_5$ bronze have been reported⁴³.

The Rietveld refinement of the XRD pattern of $Zn_{0.41}V_2O_5$ is reported in **Figure 8a**, for which soft M-O (M = V, Zn) distance restraints were imposed. Crystallographic data and atomic positions of $Zn_{0.41}V_2O_5$ are gathered in **Tables 1** and **2**, respectively. Even if caution should be taken regarding the accuracy of atomic positions due to the mean quality of the data obtained on composite electrodes, it is clear that Zn is placed in the interlayer space, in the same $4c$ position as

1
2
3
4 Na in γ -Na_{0.96}V₂O₅²⁶ and Li in γ -LiV₂O₅⁴⁴. In Zn_{0.41}V₂O₅, Zn is characterized by a distorted
5
6
7 octahedral coordination with an average Zn-O distance of 2.238(3)Å. This is in agreement with
8
9
10 the expected environment for CN 6 and mean bond length of 2.11 Å⁴⁵. The deconvolution of the
11
12
13 Raman spectrum (**Figure 8b**) clearly shows the apical V=O stretching modes are seen at lower
14
15
16 frequencies (957/993 cm⁻¹) as a result of the lengthening of these bonds in the Zn bronze, as
17
18
19 reported in **Table 2**. In the electroformed zinc bronze, the ZnO₆ octahedra share edges to form
20
21
22 chains running along the [010] direction (**Figure 9**). The valence states of the vanadium ions have
23
24
25 been estimated using the bond valence sum (BVS) method³⁵ (**Table 1**). The obtained values point
26
27
28 to different oxidation states between the two inequivalent vanadium sites. Indeed, V_a site is filled
29
30
31 by V⁺⁵ ions (BVS value = 4.97) while V_b site accommodates V⁺⁴ species (BVS value = 4.00),
32
33
34 which suggests that the V_b site is the redox center. This result reveals a localized character of
35
36
37 electron, comparable to that also observed in vanadium bronzes with γ -type puckered layer
38
39
40 structure such as γ -LiV₂O₅ and γ -Na_{0.96}V₂O₅²⁶ (see also values reported in Table 2).
41
42
43

44 **4. Conclusions**

45
46
47 In this work, the electrochemical properties of the γ' -V₂O₅ polymorph as a cathode material for a
48
49
50 rechargeable non-aqueous Zn-ion battery are reported for the first time. We demonstrate that despite its
51
52
53 high charge density, Zn²⁺ ions can be electrochemically accommodated in the γ' -V₂O₅ host lattice
54
55
56 through a solid solution process in line with the sloping discharge profile centered near 0.9 V vs Zn²⁺/Zn.
57
58
59
60

1
2
3 The discharge product corresponds to a new zinc vanadate bronze with composition $\text{Zn}_{0.41}\text{V}_2\text{O}_5$, whose
4 refined structure reveals only modest structural changes. The present results highlight the flexibility of
5 the puckered layered γ' - V_2O_5 structure undergoing a limited interlayer expansion (6.4%) on Zn insertion,
6 similar to that induced upon lithiation, along with minor impacts in the V_2O_5 planes. A highly reversible
7 extraction of Zn^{2+} ions accompanied by a complete structural restoration of the pristine oxide during the
8 charge process is found, revealing γ' - V_2O_5 behaves as a genuine Zn intercalation compound. Such
9 properties enable a long cycle life at moderate rate, with stable capacities around 130 mAh g^{-1} available
10 at 0.9 V over at least 60 cycles. The unique intercalation properties offered by γ' - V_2O_5 are definitively
11 illustrated by two major remarkable findings. First, the peculiar γ' - V_2O_5 structure promotes Zn insertion
12 in comparison with the difficult insertion reaction found in α - V_2O_5 , occurring at lower potential and
13 involving a poor capacity limited to one quarter that of γ' - V_2O_5 . More importantly is the astonishing
14 high working voltage of 0.9 V vs Zn^{2+}/Zn ($\approx 3.18 \text{ V vs Li}^+/\text{Li}$) exhibited by γ' - V_2O_5 . Indeed, this
15 potential value very close to that obtained for Li^+ , Na^+ and K^+ makes γ' - V_2O_5 a unique host material in
16 the field of intercalation chemistry with promising features as cathode material for “beyond Li” batteries.
17
18
19
20
21
22
23
24
25
26
27
28
29
30
31
32
33
34
35
36
37
38
39
40
41
42
43
44
45
46
47
48
49
50
51
52
53
54
55
56
57
58
59
60

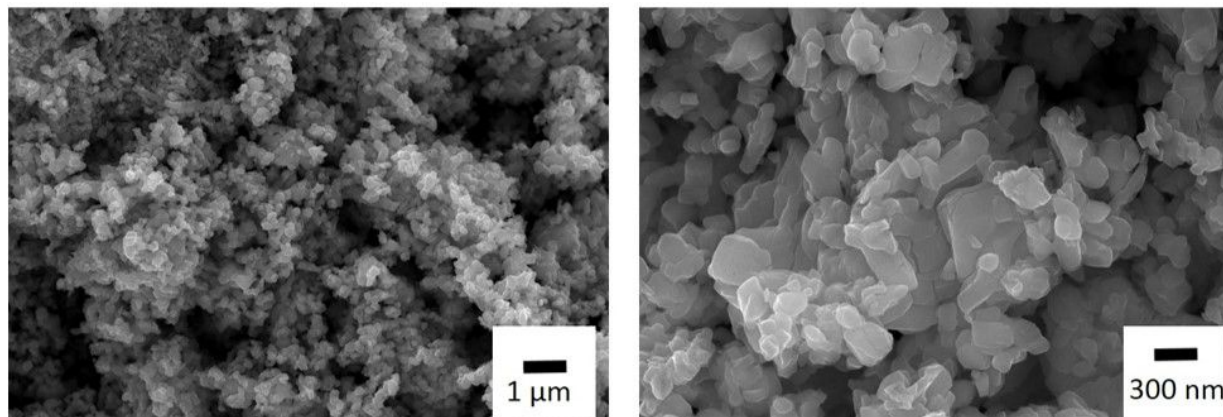


Figure 1. SEM micrographs of the as-prepared γ' - V_2O_5 powder.

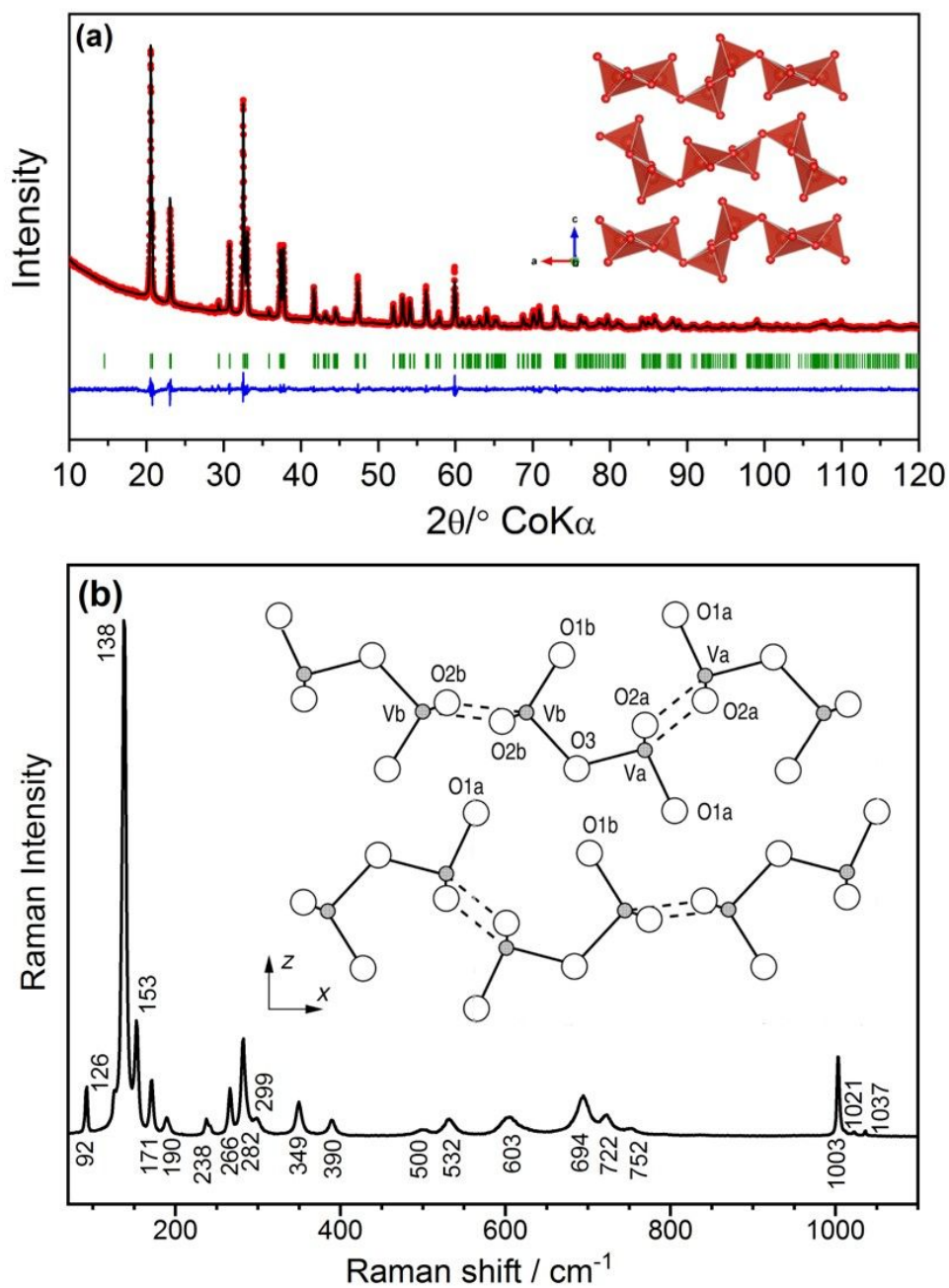


Figure 2. (a): Rietveld refinement of the XRD pattern of γ' - V_2O_5 . The red crosses, black line, and green line represent the observed, calculated and difference patterns, respectively. The positions of the Bragg reflections are shown as vertical blue bars. Inset: crystal structure of γ' - V_2O_5 (b) Raman spectrum of γ' - V_2O_5 . Inset: projection of the structure of γ' - V_2O_5 along the b -crystallographic direction showing all the V–O contacts. Dashed lines show V–O inter-chain ladder-step bonds.

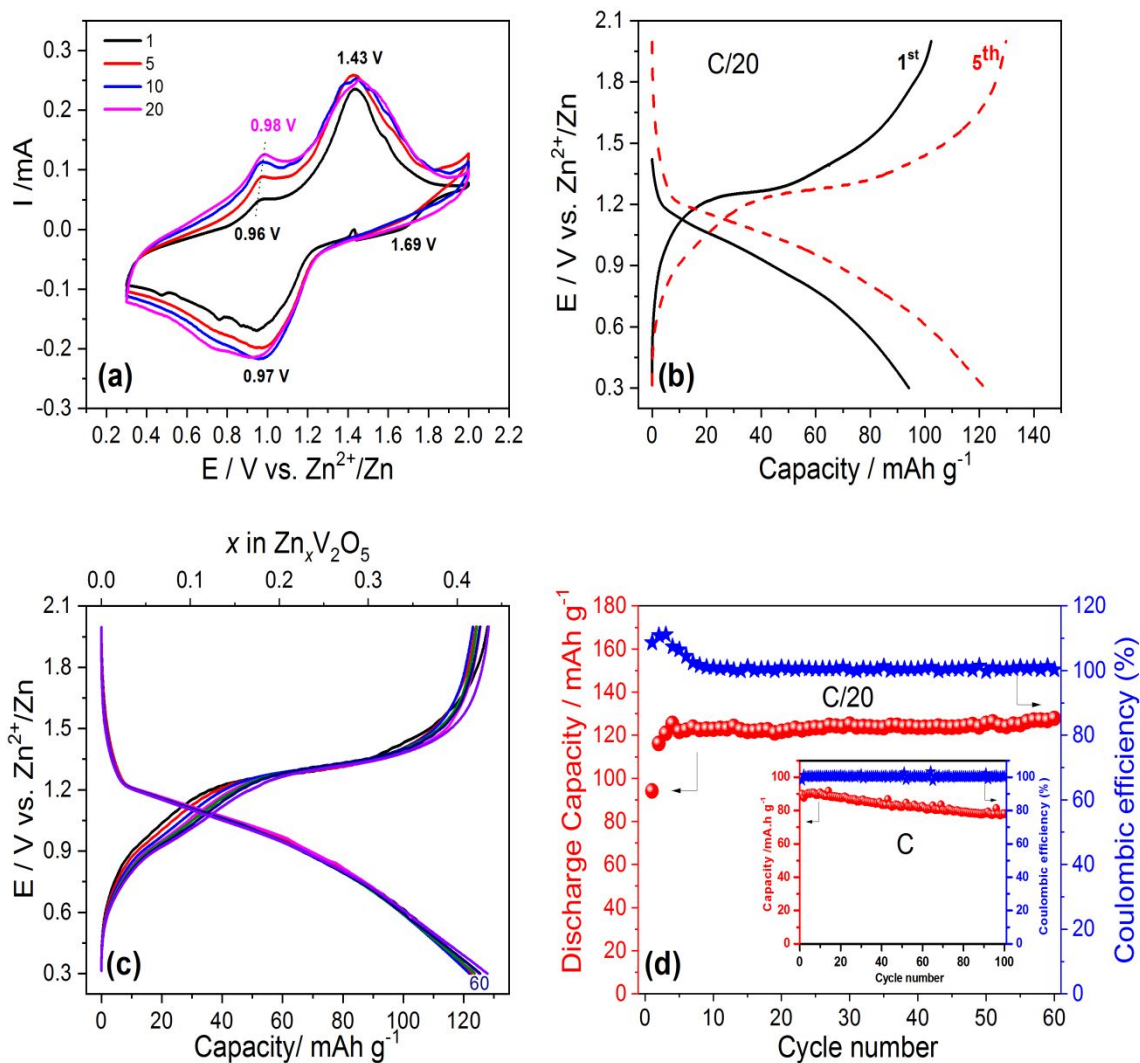


Figure 3. Electrochemical performance of γ' - V_2O_5 (a) CV curves at 0.1 mV s^{-1} ; (b) First and 5th discharge-charge cycles at $C/20$ rate (c) Discharge-charge cycles from cycle 6 to 60 (d) Evolution of the specific capacity with cycles at $C/20$ and 1C rate; 2 V – 0.3 V voltage window. Electrolyte 0.3 M $\text{Zn}(\text{OTf})_2$ in AN.

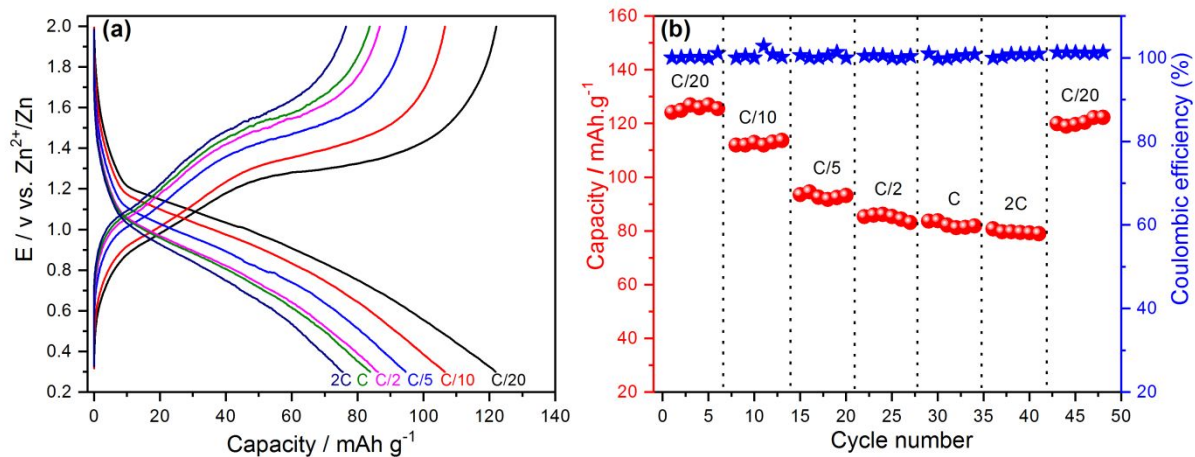


Figure 4. Rate capability study of γ -V₂O₅ in the 2 V – 0.3 V voltage window. Electrolyte 0.3 M Zn(OTf)₂ in AN.

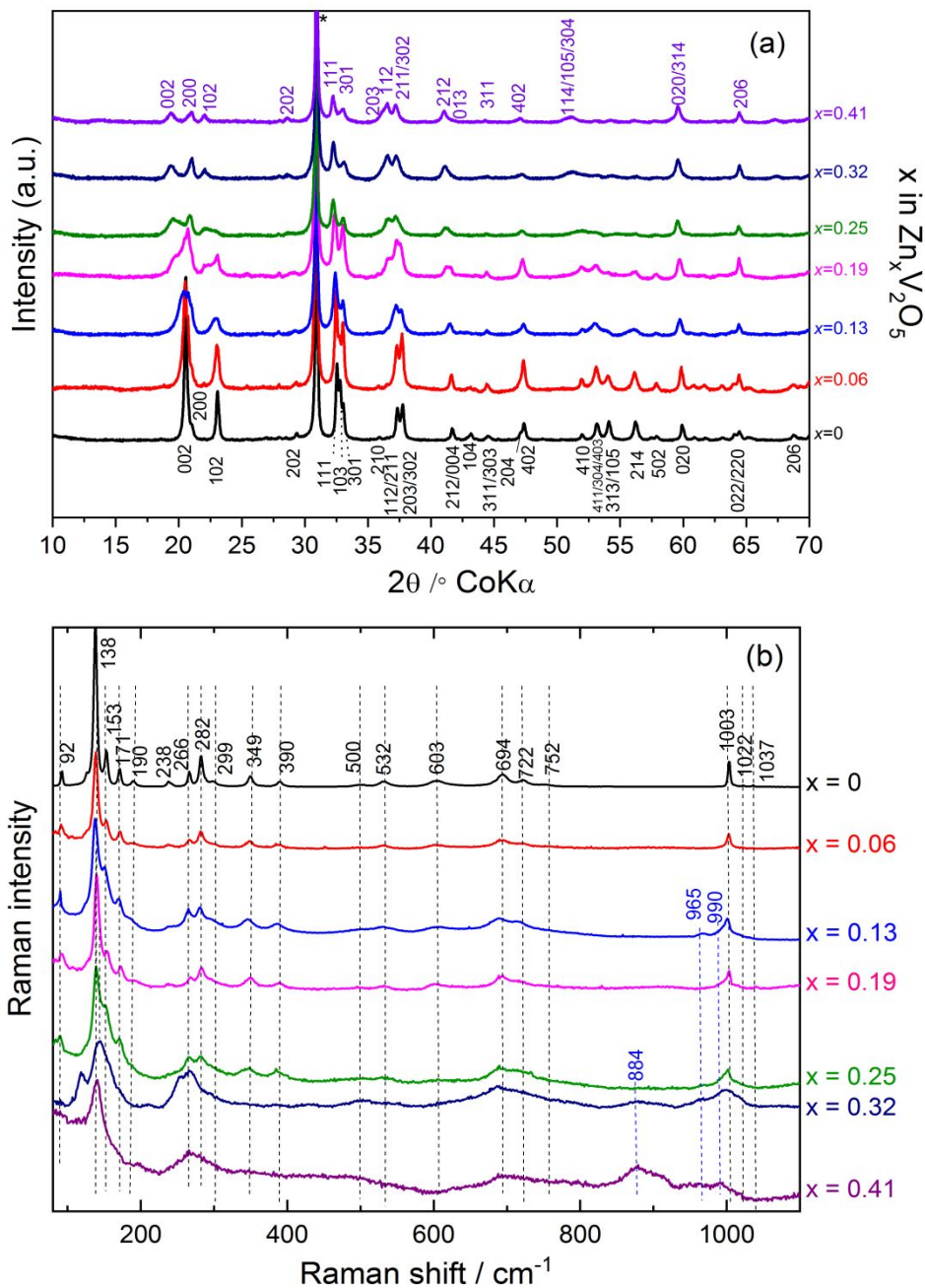


Figure 5. (a) XRD patterns and (b) Raman spectra of reduced $Zn_xV_2O_5$ electrodes ($0 \leq x \leq 0.41$).

*: Graphite reflection.

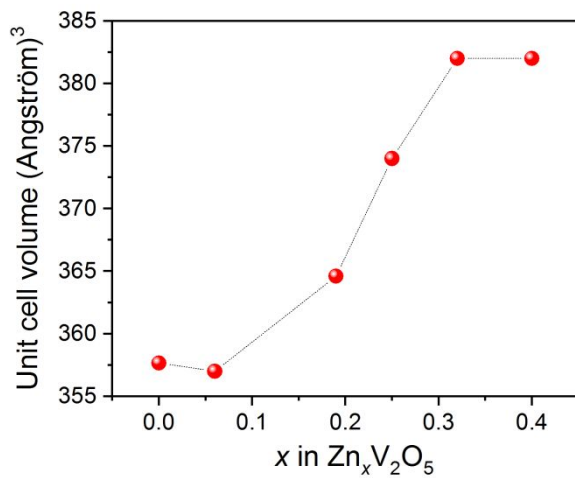


Figure 6. Variation of the unit cell volume as a function of x in Zn_xV₂O₅ electrodes ($0 \leq x \leq 0.41$).

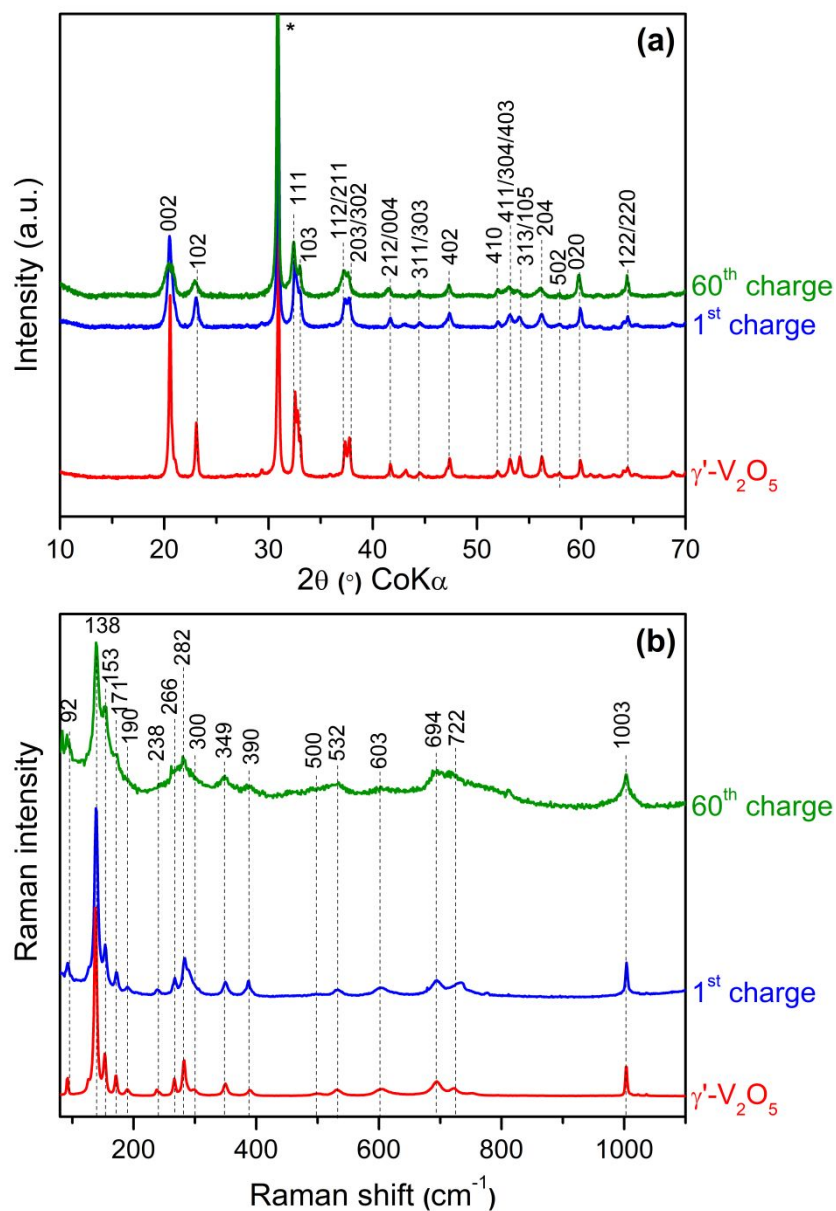


Figure 7. (a) XRD patterns and (b) Raman spectra of initial electrode, after 1st charge at C/20 and after 60 cycles at C/10. 2.0 V – 0.3 V voltage window. *: Graphite reflection

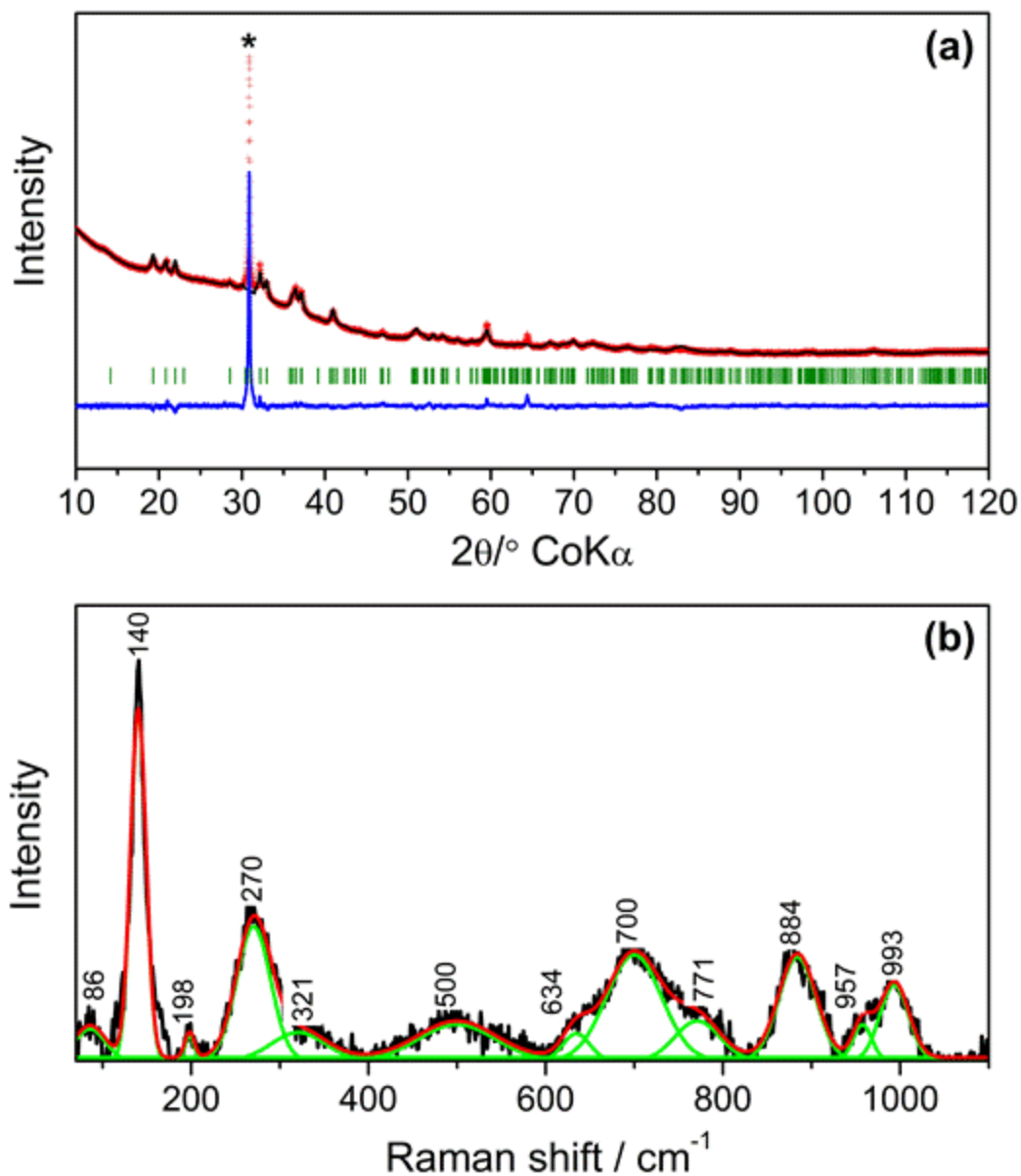


Figure 8. (a) Rietveld refinement of the X-Ray diffraction pattern of $\text{Zn}_{0.41}\text{V}_2\text{O}_5$. The red crosses, black line, and blue line represent the observed, calculated and difference patterns, respectively. The positions of the Bragg reflections are shown as vertical green bars. (b) Raman spectrum of $\text{Zn}_{0.41}\text{V}_2\text{O}_5$ with the band deconvolution shown below (in green). *: Graphite reflection.

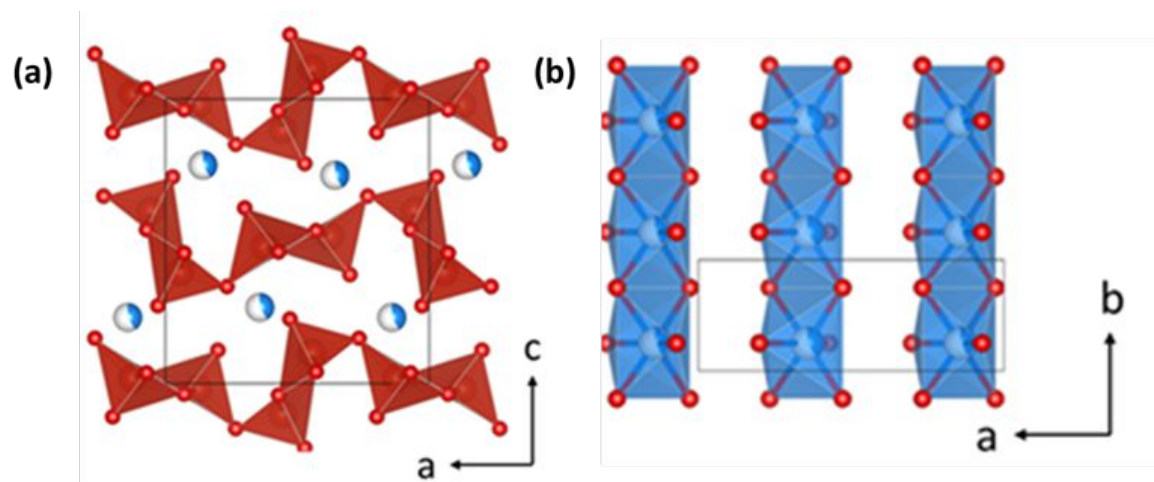


Figure 9. (a) Structure of $\text{Zn}_{0.41}\text{V}_2\text{O}_5$ phase. VO_5 pyramids are red, and blue/white spheres represent Zn atoms and vacancies, respectively (b) ZnO_6 octahedra sharing edges to form chains running along the $[010]$ direction

1
2
3 ASSOCIATED CONTENT
4
5
6
7

8 Supporting Information
9

10 This material is available free of charge via the Internet at <http://pubs.acs.org>. Crystallographic
11 data and atomic positions of γ' -V₂O₅ deduced from the Rietveld refinement of its X-ray powder
12 diffraction pattern, V-O bond lengths (in Å) extracted from the Rietveld refinement of γ' -V₂O₅;
13 Compared electrochemical properties of γ' -V₂O₅ as conventional composite electrode and
14 composite electrode with CNTs; Compared electrochemical properties of γ' -V₂O₅ and α -V₂O₅ –
15 CV, 1st galvanostatic cycle at C/20, evolution of the discharge capacity upon cycling at C/20 rate.
16
17
18
19
20
21
22
23
24
25
26
27

28 AUTHOR INFORMATION
29

30 Corresponding Author
31

32 *Rita Baddour-Hadjean (baddour@icmpe.cnrs.fr)
33
34
35
36
37

38 Author Contributions
39

40 The manuscript was written through contributions of all authors. / All authors have given approval
41 to the final version of the manuscript
42
43
44
45
46
47

48 Funding Sources
49

50 French ANR project “CASSIOPE” N° 17-CE09-0016-03
51
52
53
54
55
56
57
58
59
60

1
2
3
4 Notes

5
6 The authors declare that they have no known competing financial interests or personal
7
8 relationships that could have appeared to influence the work reported in this paper.
9

10
11
12
13 ACKNOWLEDGMENT

14
15
16 One of the author wishes to thank the French ANR project “CASSIOPE” N°17-CE09 0016-03
17
18 for its financial support. All the authors would like to thank Rémy Pires Brazuna (ICMPE-
19
20 CNRS) for his valuable contribution in SEM-EDS analysis.
21
22
23
24
25
26
27
28
29
30
31
32
33
34
35
36
37
38
39
40
41
42
43
44
45
46
47
48
49
50
51
52
53
54
55
56
57
58
59
60

TABLES

<i>Space group P n m a</i>		$R_{\text{Bragg}} = 16.1 \%$				
		$\chi^2 = 3.32$				
$V = 381.45(8) \text{ \AA}^3$		$a = 9.9053(7) \text{ \AA}, b = 3.60501(20) \text{ \AA}, c = 10.6822(9) \text{ \AA}$				
		$\alpha = \beta = \gamma = 90^\circ$				
Atom	Wyckoff position	x/a	y/b	z/c	Occupancy	BVS
V _a	4c	0.054950(8)	1/4	0.607459(8)	1	4.970(10)
V _b	4c	0.375842(9)	1/4	0.519349(7)	1	4.005(3)
O _{1a}	4c	0.47209(5)	1/4	0.77325(3)	1	2.404(3)
O _{1b}	4c	0.3009(10)	1/4	0.3828(5)	1	1.583(3)
O _{2a}	4c	0.42863(3)	1/4	0.04110(2)	1	1.922(2)
O _{2b}	4c	0.571213(18)	1/4	0.46258(5)	1	2.139(2)
O ₃	4c	0.2336(3)	1/4	0.6589(10)	1	1.515(15)
Zn	4c	0.1422(8)	1/4	0.2323(7)	0.41*	1.436(11)

Table 1. Crystallographic data and atomic positions of $\gamma\text{-Zn}_{0.41}\text{V}_2\text{O}_5$ deduced from the Rietveld refinement of its X-ray powder diffraction pattern. Results from Bond Valence Sum (BVS) analyses are listed in the last columns. * : not refined

Phases		γ' -V ₂ O ₅ (<i>Pnma</i>)	γ -LiV ₂ O ₅ (<i>Pnma</i>)	γ -Zn _{0.41} V ₂ O ₅ (<i>Pnma</i>)
Unit cell parameters and volume		$a = 9.94387(9) \text{ \AA}$ $b = 3.58389(3) \text{ \AA}$ $c = 10.03601(9) \text{ \AA}$ $V = 357.661(6) \text{ \AA}^3$	$a = 9.6947(2) \text{ \AA}$ $b = 3.6062(1) \text{ \AA}$ $c = 10.6780(2) \text{ \AA}$ $V = 373.32(2) \text{ \AA}^3$	$a = 9.9053(7) \text{ \AA}$ $b = 3.60501(20) \text{ \AA}$ $c = 10.6822(9) \text{ \AA}$ $V = 381.45(8) \text{ \AA}^3$
(V _a)O ₅	V _a -O _{1a}	1.580(5)	1.595	1.5157(4)
	V _a -O ₃	1.763(6)	1.737	1.853(4)

	V_a-O_{2a} (x2)	1.891(2)	1.892	1.9437(1)
	$(V_a-O_{2a})LS$	1.960(5)	1.975	2.0209(3)
	Average V_a-O	1.8172(19)	1.818	1.8554(4)
	BVS V_a	+5.29	+5.15	+4.97
$(V_b)O_5$	V_b-O_{1b}	1.567(5)	1.576	1.637(7)
	V_b-O_3	1.809(6)	1.961	2.051(8)
	V_b-O_{2b} (x2)	1.877(2)	1.937	1.8871(1)
	$(V_b-O_{2b})LS$	2.027(4)	1.967	2.0280(2)
	Average V_b-O	1.8315(18)	1.876	1.8980(21)
	BVS V_b	+4.99	+4.30	+4.00
$(Li, Zn)O_6$	$(M)-O_{2b}$	-----	2.047	2.197(7)
	$(M)-O_{1b}$	-----	2.044	2.248(11)
	$(M)-O_3$ (x2)	-----	2.226	2.319(6)
	$(M)-O_{1a}$ (x2)	-----	2.357	2.173(5)
	Average $(Li, Zn)-O$		2.2095	2.2383(29)

Table 2. V-O and Zn-O bond lengths in $Zn_{0.41}V_2O_5$ deduced from Rietveld refinement of its X-ray powder diffraction pattern. V-O bond lengths values in γ' - V_2O_5 and γ - LiV_2O_5 (from [25]) are also reported for comparison. LS: V-O inter-chain ladder-step bonds, indicated by dashed lines in insert of Fig. 2b.

Electrode history	F mol ⁻¹	x in Zn _x V ₂ O ₅ (EC)	Zn/V (EDS)	x in Zn _x V ₂ O ₅ (EDS)
1 st partial discharge (2.25 h at C/20)	0.12	0.06	0.025	0.050
1 st partial discharge (5 h at C/20)	0.25	0.13	0.062	0.124
1 st partial discharge (10 h at C/20)	0.50	0.25	0.119	0.238
1 st complete discharge at C/20	0.64	0.32	0.150	0.300
5 th complete discharge at C/20	0.82	0.41	0.200	0.400
After the first complete discharge-charge cycle at C/20	0	0	0.010	0.020

Table 3. Zn/V ratios in different electrodes from EDS analysis and electrochemistry (EC).

REFERENCES

- (1) Kundu, D.; Adams, B. D.; Duffort, V.; Vajargah, S. H.; Nazar, L. F. A High-Capacity and Long-Life Aqueous Rechargeable Zinc Battery Using a Metal Oxide Intercalation Cathode. *Nat. Energy* **2016**, *1*(10), 1–8, DOI:10.1038/nenergy.2016.119.
- (2) Pan, H.; Shao, Y.; Yan, P.; Cheng, Y.; Han, K. S.; Nie, Z.; Wang, C.; Yang, J.; Li, X.; Bhattacharya, P.; Mueller, K. T.; Liu, J. Reversible Aqueous Zinc/Manganese Oxide Energy Storage from Conversion Reactions. *Nat. Energy* **2016**, *1*(5), 1–7, DOI:10.1038/nenergy.2016.39.
- (3) Wan, F.; Zhang, L.; Dai, X.; Wang, X.; Niu, Z.; Chen, J. Aqueous Rechargeable Zinc/Sodium Vanadate Batteries with Enhanced Performance from Simultaneous Insertion of Dual Carriers. *Nat. Commun.* **2018**, *9*(1), 1–11, DOI:10.1038/s41467-018-04060-8.
- (4) Konarov, A.; Voronina, N.; Jo, J. H.; Bakenov, Z.; Sun, Y.-K.; Myung, S.-T. Present and Future Perspective on Electrode Materials for Rechargeable Zinc-Ion Batteries. *ACS Energy Lett.* **2018**, *3*(10), 2620–2640, DOI:10.1021/acsenergylett.8b01552.
- (5) Han, S.-D.; Rajput, N. N.; Qu, X.; Pan, B.; He, M.; Ferrandon, M. S.; Liao, C.; Persson, K.

- 1
2
3
4 A.; Burrell, A. K. Origin of Electrochemical, Structural, and Transport Properties in
5
6
7 Nonaqueous Zinc Electrolytes. *ACS Appl. Mater. Interfaces* **2016**, *8* (5), 3021–3031,
8
9
10 DOI:10.1021/acsami.5b10024.
11
12
13
14 (6) Ming, J.; Guo, J.; Xia, C.; Wang, W.; Alshareef, H. N. Zinc-Ion Batteries: Materials,
15
16
17 Mechanisms, and Applications. *Mater. Sci. Eng. R Reports* **2019**, *135*, 58–84,
18
19
20
21 DOI:10.1016/j.mser.2018.10.002.
22
23
24
25 (7) Fang, G.; Zhou, J.; Pan, A.; Liang, S. Recent Advances in Aqueous Zinc-Ion Batteries. *ACS*
26
27
28 *Energy Lett.* **2018**, *3* (10), 2480–2501, DOI:10.1021/acsenergylett.8b01426.
29
30
31
32
33 (8) Gocke, E.; Schramm, W.; Dolscheid, P.; Schöllhorn, R. Molybdenum Cluster
34
35
36 Chalcogenides Mo₆X₈: Electrochemical Intercalation of Closed Shell Ions Zn²⁺, Cd²⁺, and
37
38
39 Na. *J. Solid State Chem.* **1987**, *70* (1), 71–81, DOI:10.1016/0022-4596(87)90179-4.
40
41
42
43
44 (9) Arroyo y de Dompablo, M. E; Morán, E ; Alario-Franco, M. Á. ; Drymiotis, F.; Bianchi, A.
45
46
47 D.; Fisk, Z. Novel superconductors obtained by electrochemical Zn intercalation of β-
48
49
50 ZrNCl and related compounds, *Int. J. Inorg. Mater.* **2000**, *2*, 581–588, DOI:10.1016/s1466-
51
52
53
54 6049(00)00087-8
55
56
57
58
59
60

- 1
2
3
4 (10) Guerfi, A.; Trottier, J.; Boyano, I.; De Meatza, I.; Blazquez, J. A.; Brewer, S.; Ryder, K. S.;
5
6
7 Vijh, A.; Zaghbi, K. High Cycling Stability of Zinc-Anode/Conducting Polymer
8
9
10 Rechargeable Battery with Non-Aqueous Electrolyte. *J. Power Sources* **2014**, *248*, 1099–
11
12
13 1104, DOI:10.1016/j.jpowsour.2013.09.082.
14
15
16
17 (11) Pan, C.; Nuzzo, R. G.; Gewirth, A. A. ZnAl_xCo_{2-x}O₄ Spinel as Cathode Materials for Non-
18
19
20 Aqueous Zn Batteries with an Open Circuit Voltage of ≤2 V. *Chem. Mater.* **2017**, *29*(21),
21
22
23 9351–9359, DOI:10.1021/acs.chemmater.7b03340.
24
25
26
27
28 (12) Pan, C.; Zhang, R.; Nuzzo, R. G.; Gewirth, A. A. ZnNi_xMn_xCo_{2-2x}O₄ Spinel as a High-
29
30
31 Voltage and High-Capacity Cathode Material for Nonaqueous Zn-Ion Batteries. *Adv.*
32
33
34 *Energy Mater.* **2018**, *8*(22), 1800589, DOI:10.1002/aenm.201800589.
35
36
37
38
39 (13) Han, S.-D.; Kim, S.; Li, D.; Petkov, V.; Yoo, H. D.; Phillips, P. J.; Wang, H.; Kim, J. J.;
40
41
42 More, K. L.; Key, B.; Klie, R. F.; Cabana, J.; Stamenkovic, V. R.; Fister, T. T.; Markovic,
43
44
45 N. M.; Burrell, A. K.; Tepavcevic, S.; Vaughey, J. T. Mechanism of Zn Insertion into
46
47
48 Nanostructured δ-MnO₂: A Nonaqueous Rechargeable Zn Metal Battery. *Chem. Mater.*
49
50
51 **2017**, *29*(11), 4874–4884, DOI:10.1021/acs.chemmater.7b00852.
52
53
54
55
56
57
58
59
60

- 1
2
3
4 (14) Senguttuvan, P.; Han, S.-D.; Kim, S.; Lipson, A. L.; Tepavcevic, S.; Fister, T. T.; Bloom,
5
6 I. D.; Burrell, A. K.; Johnson, C. S. A High Power Rechargeable Nonaqueous Multivalent
7
8 Zn/V₂O₅ Battery. *Adv. Energy Mater.* **2016**, *6* (24), 1600826,
9
10
11
12
13
14 DOI:10.1002/aenm.201600826.
15
16
17
18 (15) Kundu, D.; Vajargah, S. H.; Wan, L.; Adams, B.; Prendergast, D.; Nazar, L. F. Aqueous vs.
19
20
21 Nonaqueous Zn-Ion Batteries: Consequences of the Desolvation Penalty at the Interface.
22
23
24
25 *Energy Environ. Sci.* **2018**, *11* (4), 881–892, DOI:10.1039/c8ee00378e.
26
27
28
29 (16) Huang, J.-Q.; Guo, X.; Lin, X.; Zhu, Y.; Zhang, B. Hybrid Aqueous/Organic Electrolytes
30
31
32 Enable the High-Performance Zn-Ion Batteries. *Research* **2019**, *2019*, 1–10,
33
34
35
36 DOI:10.34133/2019/2635310.
37
38
39
40 (17) Chen, D.; Rui, X.; Zhang, Q.; Geng, H.; Gan, L.; Zhang, W.; Li, C.; Huang, S.; Yu, Y.
41
42
43 Persistent Zinc-Ion Storage in Mass-Produced V₂O₅ Architectures. *Nano Energy* **2019**, *60*,
44
45
46
47 171–178, DOI:10.1016/j.nanoen.2019.03.034.
48
49
50
51 (18) Cocciantelli, J. M.; Doumerc, J. P.; Pouchard, M.; Broussely, M.; Labat, J. Crystal
52
53
54 Chemistry of Electrochemically Inserted Li_xV₂O₅. *J. Power Sources* **1991**, *34*(2), 103–111,
55
56
57
58
59
60

1
2
3
4 DOI:10.1016/0378-7753(91)85029-v.
5
6
7

8 (19) Parija, A.; Prendergast, D.; Banerjee, S. Evaluation of Multivalent Cation Insertion in
9
10 Single- and Double-Layered Polymorphs of V_2O_5 . *ACS Appl. Mater. Interfaces* **2017**, *9*
11
12 (28), 23756–23765, DOI:10.1021/acsami.7b05556.
13
14
15
16

17
18 (20) Parija, A.; Liang, Y.; Andrews, J. L.; Jesus, L. R. De; Prendergast, D.; Banerjee, S.
19
20 Topochemically De-Intercalated Phases of V_2O_5 as Cathode Materials for Multivalent
21
22 Intercalation Batteries: A First-Principles Evaluation. *Chem. Mater.* **2016**, *28* (16), 5611–
23
24
25
26
27
28
29 5620, DOI:10.1021/acs.chemmater.6b01006.
30
31

32
33 (21) Baddour-Hadjean, R.; Safrany Renard, M.; Pereira-Ramos, J. P. Unraveling the Structural
34
35 Mechanism of Li Insertion in γ' - V_2O_5 and Its Effect on Cycling Properties. *Acta Mater.*
36
37
38
39
40
41
42
43
44
45
46
47
48
49
50
51
52
53
54
55
56
57
58
59
60
2019, *165*, 183–191, DOI:10.1016/j.actamat.2018.11.043.

61
62
63
64
65
66
67
68
69
70
71
72
73
74
75
76
77
78
79
80
81
82
83
84
85
86
87
88
89
90
91
92
93
94
95
96
97
98
99
100
101
102
103
104
105
106
107
108
109
110
111
112
113
114
115
116
117
118
119
120
121
122
123
124
125
126
127
128
129
130
131
132
133
134
135
136
137
138
139
140
141
142
143
144
145
146
147
148
149
150
151
152
153
154
155
156
157
158
159
160
161
162
163
164
165
166
167
168
169
170
171
172
173
174
175
176
177
178
179
180
181
182
183
184
185
186
187
188
189
190
191
192
193
194
195
196
197
198
199
200
201
202
203
204
205
206
207
208
209
210
211
212
213
214
215
216
217
218
219
220
221
222
223
224
225
226
227
228
229
230
231
232
233
234
235
236
237
238
239
240
241
242
243
244
245
246
247
248
249
250
251
252
253
254
255
256
257
258
259
260
261
262
263
264
265
266
267
268
269
270
271
272
273
274
275
276
277
278
279
280
281
282
283
284
285
286
287
288
289
290
291
292
293
294
295
296
297
298
299
300
301
302
303
304
305
306
307
308
309
310
311
312
313
314
315
316
317
318
319
320
321
322
323
324
325
326
327
328
329
330
331
332
333
334
335
336
337
338
339
340
341
342
343
344
345
346
347
348
349
350
351
352
353
354
355
356
357
358
359
360
361
362
363
364
365
366
367
368
369
370
371
372
373
374
375
376
377
378
379
380
381
382
383
384
385
386
387
388
389
390
391
392
393
394
395
396
397
398
399
400
401
402
403
404
405
406
407
408
409
410
411
412
413
414
415
416
417
418
419
420
421
422
423
424
425
426
427
428
429
430
431
432
433
434
435
436
437
438
439
440
441
442
443
444
445
446
447
448
449
450
451
452
453
454
455
456
457
458
459
460
461
462
463
464
465
466
467
468
469
470
471
472
473
474
475
476
477
478
479
480
481
482
483
484
485
486
487
488
489
490
491
492
493
494
495
496
497
498
499
500
501
502
503
504
505
506
507
508
509
510
511
512
513
514
515
516
517
518
519
520
521
522
523
524
525
526
527
528
529
530
531
532
533
534
535
536
537
538
539
540
541
542
543
544
545
546
547
548
549
550
551
552
553
554
555
556
557
558
559
560
561
562
563
564
565
566
567
568
569
570
571
572
573
574
575
576
577
578
579
580
581
582
583
584
585
586
587
588
589
590
591
592
593
594
595
596
597
598
599
600
601
602
603
604
605
606
607
608
609
610
611
612
613
614
615
616
617
618
619
620
621
622
623
624
625
626
627
628
629
630
631
632
633
634
635
636
637
638
639
640
641
642
643
644
645
646
647
648
649
650
651
652
653
654
655
656
657
658
659
660
661
662
663
664
665
666
667
668
669
670
671
672
673
674
675
676
677
678
679
680
681
682
683
684
685
686
687
688
689
690
691
692
693
694
695
696
697
698
699
700
701
702
703
704
705
706
707
708
709
710
711
712
713
714
715
716
717
718
719
720
721
722
723
724
725
726
727
728
729
730
731
732
733
734
735
736
737
738
739
740
741
742
743
744
745
746
747
748
749
750
751
752
753
754
755
756
757
758
759
760
761
762
763
764
765
766
767
768
769
770
771
772
773
774
775
776
777
778
779
780
781
782
783
784
785
786
787
788
789
790
791
792
793
794
795
796
797
798
799
800
801
802
803
804
805
806
807
808
809
810
811
812
813
814
815
816
817
818
819
820
821
822
823
824
825
826
827
828
829
830
831
832
833
834
835
836
837
838
839
840
841
842
843
844
845
846
847
848
849
850
851
852
853
854
855
856
857
858
859
860
861
862
863
864
865
866
867
868
869
870
871
872
873
874
875
876
877
878
879
880
881
882
883
884
885
886
887
888
889
890
891
892
893
894
895
896
897
898
899
900
901
902
903
904
905
906
907
908
909
910
911
912
913
914
915
916
917
918
919
920
921
922
923
924
925
926
927
928
929
930
931
932
933
934
935
936
937
938
939
940
941
942
943
944
945
946
947
948
949
950
951
952
953
954
955
956
957
958
959
960
961
962
963
964
965
966
967
968
969
970
971
972
973
974
975
976
977
978
979
980
981
982
983
984
985
986
987
988
989
990
991
992
993
994
995
996
997
998
999
1000

(22) Baddour-Hadjean, R.; Renard, M. S.; Pereira-Ramos, J. P. Kinetic Insight into the
Electrochemical Lithium Insertion Process in the Puckered-Layer γ' - V_2O_5 Polymorph. *J.*
Electrochem. Soc. **2019**, *166* (14), A3474, DOI:10.1149/2.1211914jes.

(23) Renard, M. S.; Emery, N.; Baddour-Hadjean, R.; Pereira-Ramos, J. P. γ' - V_2O_5 : A New

- 1
2
3
4 High Voltage Cathode Material for Sodium-Ion Battery. *Electrochim. Acta* **2017**, *252*, 4–
5
6
7 11, DOI:10.1016/j.electacta.2017.08.175.
8
9
10
11 (24) Safrany Renard, M.; Baddour-Hadjean, R.; Pereira-Ramos, J. P. Kinetic Insight into the
12
13
14 Electrochemical Sodium Insertion-Extraction Mechanism of the Puckered γ' -V₂O₅
15
16
17 Polymorph. *Electrochim. Acta* **2019**, *322*, 134670, DOI:10.1016/j.electacta.2019.134670.
18
19
20
21
22 (25) Baddour-Hadjean, R.; Safrany Renard, M.; Pereira-Ramos, J. P. Enhanced Electrochemical
23
24
25 Properties of Ball-Milled γ' -V₂O₅ as Cathode Material for Na-Ion Batteries: A Structural
26
27
28 and Kinetic Investigation. *J. Power Sources* **2021**, *482*, 229017,
29
30
31 DOI:10.1016/j.jpowsour.2020.229017.
32
33
34
35
36 (26) Emery, N.; Baddour-Hadjean, R.; Batyrbekuly, D.; Laïk, B.; Bakenov, Z.; Pereira-Ramos,
37
38
39 J.-P. γ -Na_{0.96}V₂O₅: A New Competitive Cathode Material for Sodium-Ion Batteries
40
41
42 Synthesized by a Soft Chemistry Route. *Chem. Mater.* **2018**, *30* (15), 5305–5314,
43
44
45 DOI:10.1021/acs.chemmater.8b02066.
46
47
48
49
50 (27) Bhatia, A.; Pereira-Ramos, J.-P.; Emery, N.; Baddour-Hadjean, R. γ' -V₂O₅ Polymorph as a
51
52
53 Promising Host Structure for Potassium Storage: An Electrochemical and Structural Study.
54
55
56
57
58
59
60

- 1
2
3
4 *Chem. Mater.* **2021**, *33* (13), 5276–5289, DOI:10.1021/acs.chemmater.1c01390.
5
6
7
- 8 (28) Muller-Bouvet, D.; Baddour-Hadjean, R.; Tanabe, M.; Huynh, L. T. N.; Le, M. L. P.;
9
10 Pereira-Ramos, J. P. Electrochemically Formed α' - NaV_2O_5 : A New Sodium Intercalation
11
12 Compound. *Electrochim. Acta* **2015**, *176*, 586–593, DOI:10.1016/j.electacta.2015.07.030.
13
14
15
16
17
- 18 (29) Baddour-Hadjean, R.; Safrany Renard, M.; Emery, N.; Huynh, L. T. N.; Le, M. L. P.;
19
20 Pereira-Ramos, J. P. The Richness of V_2O_5 Polymorphs as Superior Cathode Materials for
21
22 Sodium Insertion. *Electrochim. Acta* **2018**, *270*, 129–137,
23
24
25
26
27
28
29 DOI:10.1016/j.electacta.2018.03.062.
30
31
- 32 (30) Delmas, C.; Cognac-Auradou, H.; Cocciantelli, J. M.; Ménétrier, M.; Doumerc, J. P. The
33
34 $\text{Li}_x\text{V}_2\text{O}_5$ System: An Overview of the Structure Modifications Induced by the Lithium
35
36 Intercalation. *Solid State Ionics* **1994**, *69* (3–4), 257–264, DOI:10.1016/0167-
37
38
39
40
41
42
43
44
45
46
47
48
49
50
51
52
53
54
55
56
57
58
59
60
- 54 *Inorg. Chem.* **2017**, *56* (3), 1734–1741, DOI:10.1021/acs.inorgchem.6b02880.

- 1
2
3
4 (32) Rietveld, H. M.; IUCr. A Profile Refinement Method for Nuclear and Magnetic Structures.
5
6
7 *urn:issn:0021-8898* **1969**, *2* (2), 65–71, DOI:10.1107/S0021889869006558.
8
9
10
11 (33) J. Rodríguez-Carvajal. FullProf Suite Homepage <https://www.ill.eu/sites/fullprof/>
12
13
14 (accessed 2021 -10 -19).
15
16
17
18 (34) Cocciantelli, J. M.; Gravereau, P.; Doumerc, J. P.; Pouchard, M.; Hagenmuller, P. On the
19
20
21
22 Preparation and Characterization of a New Polymorph of V₂O₅. *J. Solid State Chem.* **1991**,
23
24
25 *93* (2), 497–502, DOI:10.1016/0022-4596(91)90323-A.
26
27
28
29 (35) Brown, I. D.; Altermatt, D. Bond-Valence Parameters Obtained from a Systematic Analysis
30
31
32
33 of the Inorganic Crystal Structure Database. *Acta Crystallogr. Sect. B* **1985**, *41* (4), 244–
34
35
36 247, DOI:10.1107/S0108768185002063.
37
38
39
40 (36) Baddour-Hadjean, R.; Smirnov, M. B.; Kazimirov, V. Y.; Smirnov, K. S.; Pereira-Ramos,
41
42
43
44 J.-P. The Raman Spectrum of the γ' -V₂O₅ Polymorph: A Combined Experimental and DFT
45
46
47 Study. *J. Raman Spectrosc.* **2015**, *46* (4), 406–412, DOI:10.1002/jrs.4660.
48
49
50
51 (37) Smirnov, M. B.; Roginskii, E. M.; Smirnov, K. S.; Baddour-Hadjean, R.; Pereira-Ramos,
52
53
54
55 J.-P. Unraveling the Structure–Raman Spectra Relationships in V₂O₅ Polymorphs via a
56
57
58
59
60

- 1
2
3
4 Comprehensive Experimental and DFT Study. *Inorg. Chem.* **2018**, *57* (15), 9190–9204,
5
6
7 DOI:10.1021/acs.inorgchem.8b01212.
8
9
10
11 (38) Frost, R. L.; Palmer, S. J.; Čejka, J.; Sejkora, J.; Plášil, J.; Bahfenne, S.; Keeffe, E. C. A
12
13
14 Raman Spectroscopic Study of the Different Vanadate Groups in Solid-State Compounds—
15
16
17 Model Case: Mineral Phases Vésigniéite [BaCu₃(VO₄)₂(OH)₂] and Volborthite
18
19 [Cu₃V₂O₇(OH)₂·2H₂O]. *J. Raman Spectrosc.* **2011**, *42* (8), 1701–1710,
20
21
22 DOI:10.1002/jrs.2906.
23
24
25
26
27
28 (39) Galy, J. Sur quelques nouvelles familles de composés non-stoechiométriques du vanadium.
29
30
31 *Thèse Dr. ès Sci. Phys. , Univ. Bordeaux 1966.*
32
33
34
35
36 (40) Hagenmuller, P.; Galy, J.; Pouchard, M.; Casalot, A. Recherches Recentes Sur Les Bronzes
37
38
39 de Vanadium II. Elements d'insertion Divalents et Trivalents. *Mater. Res. Bull.* **1966**, *1* (2),
40
41
42 95–107, DOI:10.1016/0025-5408(66)90003-1.
43
44
45
46
47 (41) Shreenivasa, L.; Yogeeshwari, R. T.; Viswanatha, R.; Sriram, G.; Kalegowda, Y.; Kurkuri,
48
49
50 M. D.; Ashoka, S. An Introduction of New Nanostructured Zn_{0.29}V₂O₅ Cathode Material for
51
52
53
54 Lithium Ion Battery: A Detailed Studies on Synthesis, Characterization and Lithium
55
56
57
58
59
60

- 1
2
3 Uptake. *Mater. Res. Express* **2019**, *6*(11), 115035, DOI:10.1088/2053-1591/ab4572.
4
5
6
7
8 (42) Li, Q.; Zhang, Q.; Liu, C.; Zhou, Z.; Li, C.; He, B.; Man, P.; Wang, X.; Yao, Y. Anchoring
9
10 V₂O₅ Nanosheets on Hierarchical Titanium Nitride Nanowire Arrays to Form Core–Shell
11
12 Heterostructures as a Superior Cathode for High-Performance Wearable Aqueous
13
14 Rechargeable Zinc-Ion Batteries. *J. Mater. Chem. A* **2019**, *7* (21), 12997–13006,
15
16 DOI:10.1039/c9ta03330k.
17
18
19
20
21
22
23
24
25 (43) Chang, L. L. Y.; Wang, F. Y. Li-(Mg,Zn,Ni) Vanadates. *J. Am. Ceram. Soc.* **1988**, *71* (8),
26
27 689–693, DOI:10.1111/j.1151-2916.1988.tb06389.x.
28
29
30
31
32
33 (44) Galy, J.; Darriet, J.; Hagenmuller, P. Li_xV₂O₅ bronzes: structure of beta'-phase and
34
35 refinement of gamma-phase structure, *Rev. Chim. Miner.* **1971**, *8*, 509-522.
36
37
38
39
40 (45) Gagné, O. C.; Hawthorne, F. C. Bond-Length Distributions for Ions Bonded to Oxygen:
41
42 Results for the Transition Metals and Quantification of the Factors Underlying Bond-Length
43
44 Variation in Inorganic Solids. *urn:issn:2052-2525* **2020**, *7* (4), 581–629,
45
46 DOI:10.1107/S2052252520005928.
47
48
49
50
51
52
53
54
55
56
57
58
59
60

TOC GRAPHIC

